Orientational ordering of polydisperse nanorods on a flat surface

Sakineh Mizani [a)], Shahab Naghavi[a)] and Szabolcs Varga [c)]

[a)]Department of Physical and Computational Chemistry, Shahid Beheshti University, 1983969411 Tehran, Iran

[c)]Physics Department, Centre for Natural Sciences, University of Pannonia, PO Box 158, Veszprém, H-8201 Hungary

Abstract

The use of two-dimensional (2D) liquid crystals made of carbon nanorods has become increasingly popular in electronic, optical, and energy applications due to their unique properties. However, the orientational ordering of such liquid crystals remains poorly understood. Here, we explore the orientational ordering aspects of two-dimensional (2D) liquid crystals made of nanorods, such as carbon nanorods, using the hard needle model, in which Onsager's theory is used to explore the impact of polydispersity on nematic ordering. Our results show that polydispersity plays a crucial role in stabilizing the nematic phase over the isotropic phase, albeit at the expense of weaker orientational ordering. Longer rods, in particular, contribute to the stabilization of the nematic phase, whereas shorter rods result in weaker nematic ordering. To achieve a highly ordered 2D nematic phase, the polydispersity of the nanorods must be reduced.

Introduction

Carbon nanotubes (CNTs) have exceptional physical and mechanical properties, outperforming all current materials in terms of high stiffness, strength, conformability, and a wide length-to-diameter ratio [1-3]. They have wide uses in electronic devices such as transistors and fuel cells, as well as in environmental and biotechnological domains because of their stunning structure, great strength, and higher thermal and electrical conductivity than diamond [4-7]. These characteristics can also be fine-tuned by altering the diameters, wall structures, chiralities, and lengths of CNTs. The exceptional mechanical properties of CNTs, paired with their low density, are expected to open up several new avenues for the development of new material systems [8-9].

The main challenge in fully utilizing the distinct properties of individual nanotubes for a variety of applications is to produce macroscopically ordered nanotube assemblies [10].

Experimental studies demonstrate that very short and very long CNTs as well as low-concentration suspensions do not produce long-range orientational alignment [11]. This limitation can be overcome by inserting them into a nematic liquid crystal host, where the mesogenic molecules have strong self-organizing abilities [12-14]. The other possible way is to collect them at the liquid-liquid interface, where the excluded volume interactions and the applied flow enhance the orientational ordering of the CNTs. In such a way a two-dimensional (2D) nematic liquid crystal can be constructed with the CNTs [15, 16]. Recent experiments have found that applying an electric field to a mixture of CNTs and liquid crystals (LC) can increase their orientational order parameters [17]. Moreover, liquid anhydrous sulfuric acid exhibits a partially ordered structure when SWNTs are present [18]. These results suggest that the process of CNT alignment is highly dependent on CNT length distribution. To address this issue, Wen et al. conducted a length-controlling experiment using three system-based technologies. Their results suggest that controlling CNTs length and distribution can significantly improve the alignment of arrays [19].

Several theoretical papers investigated the phase behavior and structural properties of carbon nanotubes (CNTs) in conjunction with LC [20, 21]. These studies explored various factors, such as the length-to-diameter ratio, composition, concentration, and electric field strength on the phase properties of LC and CNTs [22-25]. The effects of CNTs on the stability of antiferroelectric liquid crystals were also studied [26]. Additionally, the percolation of thin colloidal nanoparticles in liquid dispersions in the presence of external orienting fields has been studied [27]. It was found that unusual re-entrance phenomena and percolation occur only in a small region of the phase diagram [27]. Regarding the electric properties of the ordered phases of nanorods, Monte Carlo simulations were used to examine the influence of nanorod length distribution and concentration on the percolation threshold [28, 29]. Moreover, several composites were studied using theory and simulation to understand the role of nanotube length distributions on electrical conductivity [30-32].

It is now well understood that the orientational ordering of anisotropic biological or synthetic nanoparticles is mainly governed by hard body excluded volume interactions [33]. However, in most cases, the suspension of synthetic nanoparticles suffers from polydispersity in length, diameter**,** or both. To include the effect of polydispersity in simulation and theoretical studies, it is widely accepted to use continuous distribution functions for the length and diameter of anisotropic nanoparticles. However, this extra parameter substantially complicates the modeling, and some simplifying assumptions are inevitable to get some information about

the change in the orientational and positional ordering of nanoparticles due to polydispersity. The most common approximations are to consider the polydispersity as a perturbation [34], restrict the orientational freedom of the particles [35-38], use the trial function method for the orientational distribution function [39-41], place the particles into a lattice [42] and use the moment free energy method [43-45]. These studies revealed the complex effect of polydispersity on the stability of mesophases and the ordering behavior of nanorods. One of the important results in length polydisperse hard rod systems is that the long rods accumulate mainly in the orientationally ordered phases, while the short ones accumulate in the isotropic one, but the isotropic-nematic transition density is weakly affected [34, 37]. In addition, the smectic and crystalline phases are suppressed, while the columnar order becomes stable [41]. It is also pointed out that polydispersity can stabilize the biaxial nematic phase [38].

The motivation of our theoretical study is the recent observation of the highly ordered 2D nematic phase of CNTs on a liquid-liquid interface, where the length-to-diameter ratio of CNTs is on the order of hundreds [15, 19]. For example, the average length of the nanorods is 500 nm, while the average diameter is only 1.5 nm in the experiment of Jinkins et al. [15]. Although the interaction between CNT particles is very complex due to the presence of anisotropic dispersive interactions, flexibility, and polydispersity, we try to understand the role of excluded volume interactions and the length of polydispersity on the stability of the 2D nematic phase using a hard needle model, where the needles are confined to a plane in both orientation and position. We assume that the needles are polydisperse in length and they are allowed to move and rotate freely on the plane without overlapping each other. We use the well-known Onsager theory of hard anisotropic particles [33]. To solve the resulting integral equation for the orientational distribution of the polydisperse needle system, we develop an optimized mixture approach for the continuous length distribution, which can be handled easily and converges to the continuum system using only a few mixture components. Our method can be applied to arbitrary length distributions, i.e., it can have a high peak or a long tail. We show that the isotropic-nematic bifurcation density is inversely proportional to the polydispersity index; the nematic phase becomes more stable but the nematic order weakens.

Theory

We examine the orientational ordering properties of the thermalized suspension of nanorods, which are free to rotate on a flat surface. To a first approximation, the suspension of nanorods is modeled as a hard needle of finite length and zero diameters, while the effects of flexibility and other interactions are neglected. As the colloidal nanorod suspensions are usually polydisperse in length, we take into account the effect of polydispersity using continuous length distributions. Applying the extension of the Onsager theory [33, 34], we determine the isotropic-nematic (IN) transition density and the ordering properties of the nematic phase. Note that the needles do not have volume, i.e., the packing fraction of the system is always zero. Therefore, only the isotropic and nematic phases are present in this system, as the perfectly ordered nematic phase of the needles behaves like the ideal gas. We present the theory for both monodisperse and polydisperse cases in the next subsections. We also present an optimized mixture method to solve the integral equation of the polydisperse case.

a) Monodisperse fluid

On the level of Onsager theory, the free energy (F) of monodisperse fluid of hard particles on a flat surface (xy plane) is a functional of the orientational distribution function (f):

$$\beta F / A = \rho \ln \rho - \rho + \rho \int_0^{\pi} d\varphi \, f(\varphi) \ln f(\varphi) + \frac{1}{2} \rho^2 \int_0^{\pi} d\varphi_1 \int_0^{\pi} d\varphi_2 \; f(\varphi_1) f(\varphi_2) A_{exc}(\varphi_1, \varphi_2), \qquad (1)$$

where $\beta = \frac{1}{k_B T}$ is the inverse temperature, A is the surface area, $\rho = N / A$ is the two-dimensional (2D) number density, N is the number of particles, and φ is the orientation angle of the main axis of the particle with respect to the *x-axis*. In Eq. (1) it is assumed that the particle has up-down symmetry, which reduces the integration in angle φ to $0 \le \varphi \le \pi$. The excluded area between two particles (A_{exc}) depends on the shape and the orientations of the particles (φ_1 and φ_2). The functional minimization of the free energy functional (Eq, (1)) with respect to f provides a self-consistent equation for the equilibrium orientational distribution function (ODF). One can get that

$$f(\varphi)=\frac{\exp\left\{-\rho\int_0^{\pi}d\varphi_2\, f(\varphi_2)A_{exc}(\varphi,\varphi_2)\right\}}{\int_0^{\pi}d\varphi_1\exp\left\{-\rho\int_0^{\pi}d\varphi_2\, f(\varphi_2)A_{exc}(\varphi_1,\varphi_2)\right\}}. \qquad (2)$$

Note that the normalization condition of ODF, which is given by $\int_0^{\pi}d\varphi\, f(\varphi)=1$, is taken into account in the derivation of this equation. One trivial solution of Eq. (2) is the isotropic distribution with $f=1/\pi$, while the other is nematic. The nematic ODF has a peak at $\varphi=0$ and π, while it has a minimum at $\varphi=\pi/2$. The degree of nematic ordering can be measured with the help of the orientational order parameter, which is defined by $S=\int_0^{\pi}d\varphi\cos(2\varphi)f(\varphi)$. This parameter is exactly zero in the isotropic phase, while it tends to one as the orientation order increases.

In the case of hard needles with length l, the excluded area between two particles is analytic and given by:

$$A_{exc}(\varphi_1,\varphi_2)=l^2\left|\sin(\varphi_1-\varphi_2)\right|, \qquad (3)$$

where φ_1 and φ_2 are the orientation angles of particles 1 and 2, respectively. We solve Eq. (2) together with Eq. (3) numerically to determine the ordering properties of hard needles as a function of surface density (ρ). To get some insight into the orientational ordering properties of the hard needle fluid, the onset of nematic ordering can be determined analytically by performing a bifurcation analysis on Eq. (2). The bifurcation analysis of hard body fluids is well-known from the work of Kayser and Ravaché [46]. In the case of 2D hard needles, one can get that $\rho_{IN}=1.5\pi/l^2$, where ρ_{IN} is the IN transition density. The isotropic distribution ($f=1/\pi$) is the only solution of Eq. (2) for $0<\rho\le\rho_{IN}$, while both isotropic and nematic solutions exist for $\rho>\rho_{IN}$. Interestingly, the nematic solution has lower free energy than the isotropic one, i.e. the nematic phase is the stable phase at higher densities. The order of IN phase transition proved to be second order using the Onsager theory [46]. Note that the IN

phase transition of 2D needle particles is even weaker and belongs to the class of Kosterlitz–Thouless (KT) continuous transitions according to the Monte Carlo simulation study of Frenkel and Eppenga [47]. Apart from this deviation, the Onsager and other mean field theories provide an accurate description of the nematic order parameter and the equation of the state of several 2D systems such as the needle, ellipse, and rectangle fluids [33, 48].

b) Polydisperse fluid

As the nanorods are generally polydisperse in length, we extend the monodisperse case to the polydisperse one in this subsection, where the polydispersity is considered to be continuous. We introduce the length-dependent density distribution $\rho(l)$, which is related to the 2D bulk density (ρ) via $\rho = \int_0^\infty dl\rho(l)$. The length dependence of the density distribution modifies both the ideal gas and the excluded volume contributions of the free energy functional (see Eq. (1)), which makes the orientational distribution function also length dependent. The straightforward generalization of Eq. (1) for length polydisperse hard rods can be written as

$$\begin{aligned}\beta F[f]/A = &\int_0^\infty dl\,\rho(l)\ln\rho(l) - \rho(l) + \int_0^\infty dl\int_0^\pi d\varphi\rho(l)f(l,\varphi)\ln f(l,\varphi) \\ &+ \frac{1}{2}\int_0^\infty dl_1\int_0^\pi d\varphi_1\int_0^\infty dl_2\int_0^\pi d\varphi_2\rho(l_1)f(l_1,\varphi_1)\rho(l_2)f(l_2,\varphi_2)A_{exc}(l_1,l_2,\varphi_1,\varphi_2)\end{aligned} \tag{4}$$

where the excluded area between a hard needle with length and orientation (l_1,φ_1) and a second one with (l_2,φ_2) is simply given by:

$$A_{exc}(l_1,l_2,\varphi_1,\varphi_2) = l_1 l_2\left|\sin(\varphi_1-\varphi_2)\right|. \tag{5}$$

A self-consistent equation for ODF of the hard needles with length l and orientation φ can be obtained via functional minimization of Eq. (4) using Eq. (5) and the normalization condition for all lengths, $\int_0^\pi d\varphi\, f(l,\varphi) = 1$. After straightforward calculations, one can get that

$$f(l,\varphi)=\frac{\exp\left\{-l\int_0^\infty dl_2\, l_2\,\rho(l_2)\int_0^\pi d\varphi_2\, f(l_2,\varphi_2)\left|\sin(\varphi-\varphi_2)\right|\right\}}{\int_0^\pi d\varphi_1 \exp\left\{-l\int_0^\infty dl_2\, l_2\,\rho(l_2)\int_0^\pi d\varphi_2\, f(l_2,\varphi_2)\left|\sin(\varphi_1-\varphi_2)\right|\right\}} \quad . \tag{6}$$

The input of this equation is the density distribution, which can be factorized as $\rho(l)=\rho g(l)$, where ρ is the usual 2D bulk density and $g(l)$ is the normalized length distribution function satisfying $\int_0^\infty dl\, g(l)=1$. To solve Eq. (6) for the equilibrium ODF we set ρ and $g(l)$. Therefore our working equation becomes

$$f(l,\varphi)=\frac{\exp\left\{-\rho l\int_0^\infty dl_2 l_2 g(l_2)\int_0^\pi d\varphi_2\, f(l_2,\varphi_2)\left|\sin(\varphi-\varphi_2)\right|\right\}}{\int_0^\pi d\varphi_1 \exp\left\{-\rho l\int_0^\infty dl_2 l_2 g(l_2)\int_0^\pi d\varphi_2\, f(l_2,\varphi_2)\left|\sin(\varphi_1-\varphi_2)\right|\right\}}. \tag{7}$$

Again the trivial solution of this equation is the isotropic distribution, since $f(l,\varphi)=1/\pi$ satisfies Eq. (7) for any density and length distribution. The non-trivial solution of Eq. (7) is nematic, which can be obtained numerically using iteration and discretizing the integrals both in length and angle. Luckily, analytical results can be obtained for the onset of nematic ordering with the extension of the monodisperse bifurcation analysis [49]. After straightforward ca1ulation it can be shown that the density of the isotropic-nematic transition occurs exactly at

$$\rho_{IN}=1.5\pi/\left\langle l^2\right\rangle, \tag{8}$$

where $\left\langle l^2\right\rangle=\int_0^\infty dl\, l^2\, g(l)$. This shows that the widening (narrowing) length distribution decreases (increases) the transition density, i.e. the nematic phase becomes more stable with respect to the isotropic one in the polydisperse case. To check the prediction of this analysis, we solve Eq. (7) numerically as a function of ρ for a given length distribution ($g(l)$) and we search for a nematic solution, which starts to bifurcate from the isotropic solution. In this process, the first step is the discretization of the length distribution. Instead of using equidistance grid size for l, we represent the continuum distribution as a n component mixture, where we make optimization for the number of components (n), the mole fraction x_i and the average length of component i, where i=1,…,n. We replace $0<l<\infty$ with $l_{\min}<l<l_{\max}$,

where the minimal and maximal lengths can be varied to get a more reliable approximation of the continuum system. The number of adjustable lengths between the minimum and maximum lengths is taken to be *n*-1. We can write a set of discretized lengths in order as follows: $l = \{l_0 = l_{\min}, l_1, ..., l_i, ..., l_n = l_{\max}\}$. As only $l_0 = l_{\min}$ and $l_n = l_{\max}$ are fixed, we search for the optimal values of $l_1, l_2, ...$ and l_{n-1} for a given *g(l)* distribution. To do this we define the mole fraction (x_i) and the average length ($\langle l \rangle_i$) of component *i* as follows:

$$x_i := \int_{l_{i-1}}^{l_i} dl\, g(l), \tag{9}$$

$$\langle l \rangle_i := \int_{l_{i-1}}^{l_i} dl\, l\, g(l) / x_i\,, \tag{10}$$

We can see that these definitions guarantee the normalization condition and provide the right average length of the needles if our $l_{\min}$ and $l_{\max}$ lengths are chosen such that $g(l_{\min}) \approx 0$ and $g(l_{\max}) \approx 0$, because $\sum_{i=1}^{n} x_i = \int_{l_{\min}}^{l_{\max}} dl\, g(l) = 1$ and $\langle l \rangle = \int_{l_{\min}}^{l_{\max}} dl\, l\, g(l) = \sum_{i=1}^{n} x_i \langle l \rangle_i$. At this point it is worth noting that we can calculate the mole fractions and the lengths of an *n* component needle mixture for a given set of $l = \{l_0 = l_{\min,} l_1, ..., l_{n-1}, l_n = l_{\max}\}$ from Eqs. (9) and (10). To find the optimal values of $l = \{l_0 = l_{\min,} l_1, ..., l_{n-1}, l_n = l_{\max}\}$ we determine the polydispersity index of the mixture and that of the continuum system, which is given by $I_p = \langle l^2 \rangle / \langle l \rangle^2$. We can write this quantity in the discrete and continuous case as follows:

$$I_p(l_{\min}, ..., l_{\max}) = \sum_{i=1}^{n} x_i \langle l \rangle_i^2 \Big/ \left(\sum_{i=1}^{n} x_i \langle l \rangle_i \right)^2, \tag{11}$$

$$I_p = \int_0^{\infty} dl\, g(l) l^2 \Big/ \left\{ \int_0^{\infty} dl\, g(l) l \right\}^2. \tag{12}$$

Note that we highlight the difference between the discrete and continuum polydispersity index by showing the $l = \{l_0 = l_{\min,} l_1, ..., l_{n-1}, l_n = l_{\max}\}$ dependence in Eq. (11). It can be shown

that Eq. (11) underestimates the polydispersity index of the continuum system (Eq. (12)). To get the best mixture representation of the system, we search for the maximum of Eq. (11) by varying the lengths. As $l_0=l_{\min}$ and $l_n=l_{\max}$ are fixed, while $l_1, \ldots, l_{n-1}$ are the free parameters, we get the following set of equations

$$\frac{\partial I_p(l_{\min},...,l_{\max})}{\partial l_i}=0,\ (i=1,...n-1) \tag{13}$$

Using Eqs. (9), (10), (11) and (13) we end up with a set of coupled equations for the discretized lengths:

$$l_i=\frac{1}{2}\left(\langle l\rangle_i+\langle l\rangle_{i+1}\right) \tag{14}$$

where $i=1....n-1$. As we have n-1 unknown lengths and n-1 equations, the numerical solution of this set of equations provides $l_1,...,l_{n-1}$. Using these optimal lengths, we can calculate the average lengths ($\langle l\rangle_1,...,\langle l\rangle_n$) and mole fractions ($x_1,..,x_n$) of the n component mixture from Eqs. (9) and (10) . No doubt, I_p of the continuum system can be reproduced by the mixture representation if $n\to\infty$. In practice, we try to get back the actual polydispersity index as accurately as possible by finding the minimum value of n.

In the *n-component* mixture representation, the equation of ODF can be obtained from Eq. (7) using the following correspondences: $l \leftrightarrow \langle l\rangle_i$ and $g \leftrightarrow x_i$. Therefore the ODF of component i with length $\langle l\rangle_i$ can be obtained from

$$f\left(\langle l\rangle_i,\varphi\right)=\frac{\exp\left\{-\rho\langle l\rangle_i\sum_{j=1}^{n}x_j\langle l\rangle_j\int_0^{\pi}d\varphi_2\, f\left(\langle l\rangle_j,\varphi_2\right)\left|\sin(\varphi-\varphi_2)\right|\right\}}{\int_0^{\pi}d\varphi_1\exp\left\{-\rho\langle l\rangle_i\sum_{j=1}^{n}x_j\langle l\rangle_j\int_0^{\pi}d\varphi_2\, f\left(\langle l\rangle_j,\varphi_2\right)\left|\sin(\varphi_1-\varphi_2)\right|\right\}}, \tag{15}$$

where i=1,..,n. We have solved these n coupled and nonlinear equations numerically using trapezoid quadrature for the integrations and the iteration method. We measure the extent of orientational ordering of component i with the usual 2D nematic order parameter as follows

$$S_i = \int_0^{\pi} d\varphi \, f\left(\langle l \rangle_i, \varphi\right) \cos(2\varphi). \tag{16}$$

From this component order parameter, we get the global nematic order parameter by taking the average of S_i, i.e. $S = \sum_{i=1}^{n} x_i S_i$. Using the average length of the rods as a unit, which is given by $\langle l \rangle = \int_0^{\infty} dl \, l \, g(l)$, the dimensionless length and density can be written as $l^* = l / \langle l \rangle$ and $\rho^* = \rho \langle l \rangle^2$, respectively. In this unit, we get that $\left\langle l^* \right\rangle = 1$, $I_p = \left\langle l^{*2} \right\rangle$, and $\rho_{IN}^* = 1.5\pi / I_p$. We use the log-normal (LN) and the Schultz-Flory (SF) distributions for the polydisperse needle system. The LN distribution function is given by

$$g\left(l^*\right) = \frac{1}{\sqrt{2\pi \ln I_p} \, l^*} \exp\left[- \frac{\left(\ln l^* + 0.5 \ln I_p\right)^2}{2 \ln I_p} \right], \tag{17}$$

which satisfies the normalization condition and $\left\langle l^* \right\rangle = 1$. The SF distribution also satisfies these conditions and can be written as

$$g\left(l^*\right) = \alpha^{\alpha} \frac{l^{*(\alpha - 1)}}{\Gamma(\alpha)} e^{-\alpha l^*}, \tag{18}$$

where $\alpha = \frac{1}{I_p - 1}$ and Γ is the Gamma function. Eqs. (17) and (18) represent peaked length distribution, where the peak is at a length between $l^*=0$ and $l^*=\infty$. Moreover, these distribution functions are zero for very short and long rods, i.e. $g(0) = 0$ and $g\left(l^* \to \infty\right) = 0$. Note that I_p cannot be larger than 2 using Eq. (18), because $g(0) > 0$ for $I_p>2$. In the next section, we present our results in reduced units for these two length distributions.

Results

We begin this section by presenting the differences between LN and SF distribution functions for the polydisperse hard needle system. Fig. 1 shows the length dependence of LN (see Eq. (17)) and that of SF (see Eq. (18)) distributions for different values of I_p. We can see that the distributions broaden with increasing I_p, because I_p =1 corresponds to the monodisperse

limit. In both cases, the position of the maximum of the length distribution function (l_m^*) moves to the direction of lower lengths with increasing I_p. It can be proved analytically that $l_m^* = 1/I_p^{3/2}$ and $l_m^* = 2 - I_p$ for LN and SF distributions, respectively. The difference between the two distributions is that the LN distribution is symmetric in log scale, while the SF is not. In addition, the decay of the SF distribution is slower on the left-hand side than that of the LN one, while the opposite trend can be seen on the right-hand side of the peak. In addition, the height of the LN distribution is larger than that of the SF distribution. Consequently, we choose $l_{\min}^* = 10^{-7}$ for the minimal length ($l_{\min}^*$) in the mixture representation of SF length distribution, while $l_{\min}^* = 10^{-3}$ is a good choice in the case of LN distribution for the studied values of I_p. The upper limit of the length ($l_{\max}^*$) is chosen to be higher in LN than in SF distribution because the decay of LN is slower than that of SF. However, this depends on the value of I_p as the distribution functions become wider with increasing I_p. We found that $l_{\max}^* = 30$ ($l_{\max}^* = 10$) is enough high for LN (SF) distribution with $I_p = 1.75$. In practice, we decreased $l_{\min}^*$ and increased $l_{\max}^*$ with increasing I_p for both distributions to get back the polydisperity index of the continuous distribution as accurately as possible in the mixture representation. The points $l_1^*, ..., l_{n-1}^*$ between $l_{\min}^*$ and $l_{\max}^*$ are the solutions of Eq. (14) using Eqs. (9) and (10) at a given value of *n*. In Fig. 2 we show the effect of discretization on the polydispersity index as a function of a number of components. We can see that the convergence of I_p to the required value is quite fast for both distributions. Therefore the optimized mixture representation is justified to study polydisperse systems because it provides the same average length and the polydispersity index as the continuous length distribution. The advantage of this method is that we must use only a few components (*n*) with

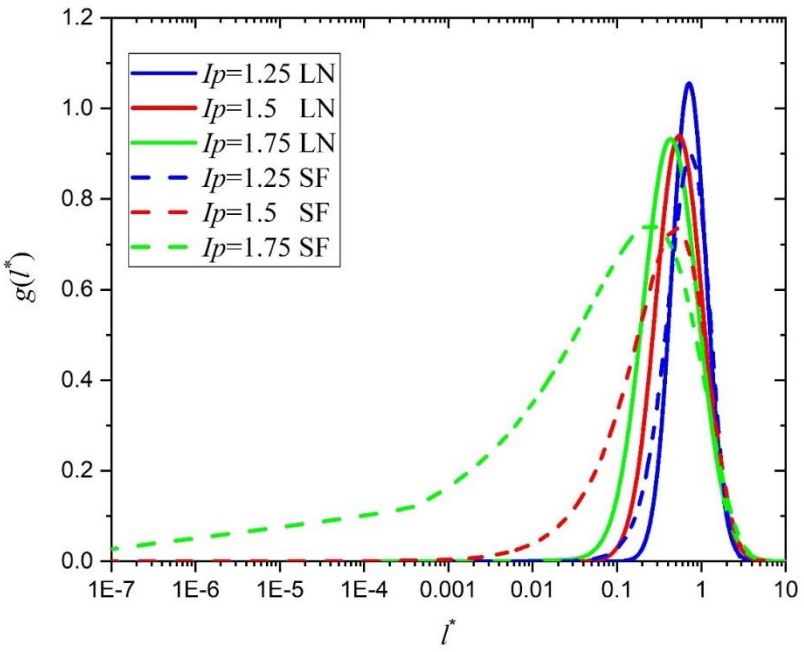

Figure 1: The effect of varying polydispersity index (I_p) on the continuous length distribution function. The SF and LN length distributions are shown as a function of dimensionless length (l^*).

given lengths ($\langle l \rangle_1,...,\langle l \rangle_n$) and mole fractions ($x_1,...,x_n$) to determine the phase behavior of polydisperse systems with continuous distribution. It can be seen in Fig. 2 that the minimal value of n depends on I_p, because more and more components are needed with increasing I_p. For example, we get I_p=1.25 with n=10 components, while n=20 is needed for I_p =1.75. The comparison of the results for LN and SF distributions shows that SF can be represented with fewer components than the LN one to reproduce the I_p value of the continuous distribution. As Eq. (15) is a set of n coupled non-linear equations for ODFs, we check the effect of n on the resulting global nematic order parameter (S). The solution of Eqs. (15) and (16) for the order parameter are shown for several values of n in Fig. 3. As the polydispersity index of the optimized mixture is slightly lower than the true value of the continuous system (see Fig. 2), the onset of the nematic ordering must occur at higher densities because $\rho_{IN}^* = 1.5\pi / I_p$ is valid for both the mixture and the continuous system. This can be seen clearly in the binary mixture representation (n=2), where the optimized mixture has a significantly lower I_p value than the prescribed one. We can see the shift of the curve to the direction of right value of ρ_{IN}^*, because I_p of the mixture converges with increasing n as shown in Fig. 2. Note that our

numerical results are always consistent with $\rho_{IN}^{*} = 1.5\pi / I_p$ for the onset of nematic ordering if we use the I_p value of the optimization. In addition, with the optimized mixture representation, the nematic order parameter is underestimated at densities below $\rho^{*} \approx 5$, while

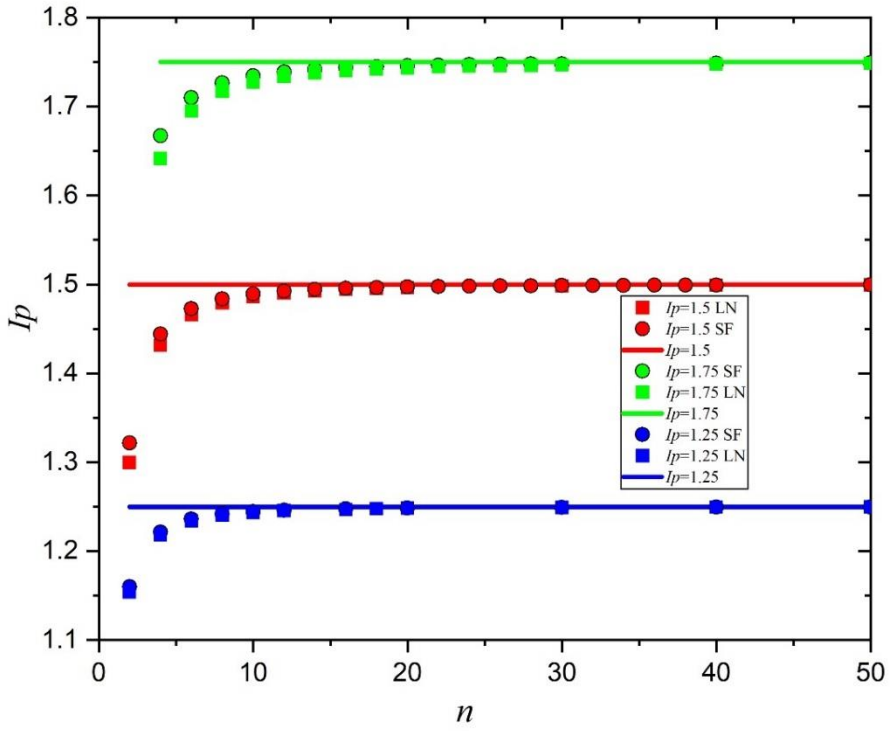

Figure 2: Polydispersity index of the optimized mixture as a function of the number of components. The square and circle symbols belong to the LN and SF distributions, respectively, while the horizontal line shows the required I_p values of the continuous distribution.

it is overestimated for higher densities. We can also see that the order parameter of the LN distribution is higher than that of the SF one for $\rho^{*}>5$. This is due to the fact that longer rods have a higher alignment ability than shorter ones, and the LN distribution contains more longer rods than the SF distribution does. As the shift between the curves is almost negligible using n=10 and n=20 components in Fig. 3 and the true value of I_p is recovered by the optimized mixture representation, we do not go beyond n=30 components even for very polydisperse cases to find the equilibrium orientation distribution function and the order parameters from Eqs. (15) and (16). The global nematic order parameter is shown as a function of 2D number density in Fig. 4 for both SF and LN length distributions. In accordance with $\rho_{IN}^{*} = 1.5\pi / I_p$

, the IN transition occurs at lower densities with increasing I_p , while $\rho^*_{IN} = 1.5\pi$ is recovered for the monodisperse case (I_p=1). Therefore, the increasing polydispersity stabilizes the

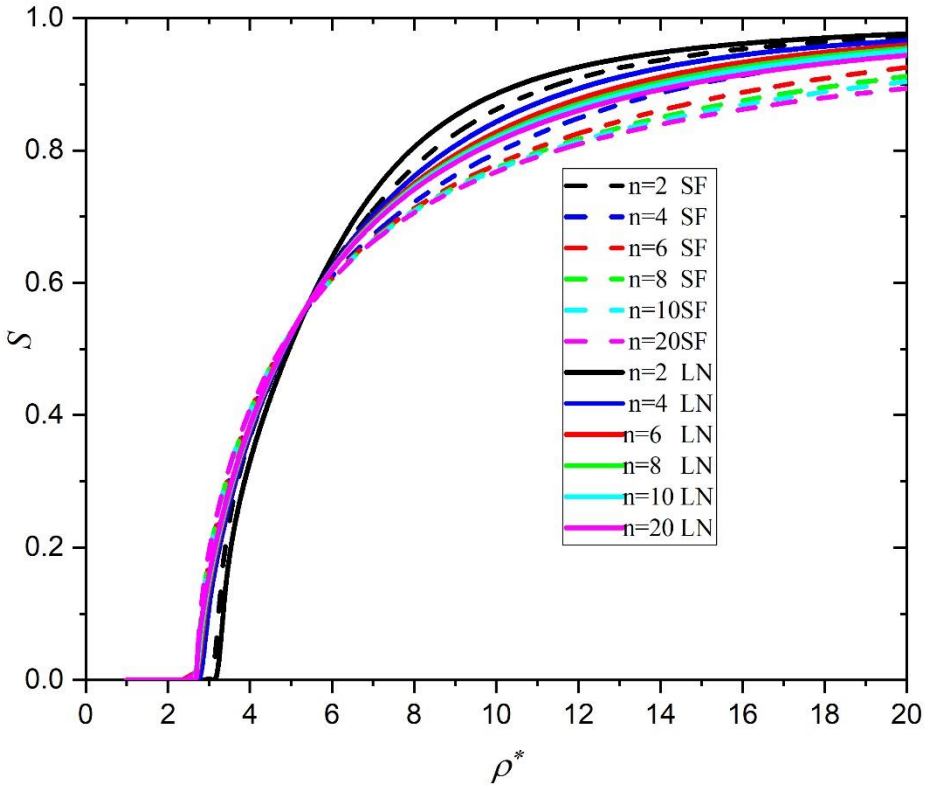

Figure 3: The effect of a number of components on the global order parameter as a function of 2D density for I_P =1.75. The solid curve indicates the results of LN length distribution, while the dashed curve represents the results coming from SF one.

nematic phase with respect to the isotropic one. This does not mean, however, that polydispersity results in a stronger nematic ordering than what occurs in the monodisperse system. We can see that the isotropic and weakly nematic phases of the monodisperse system with S<0.6 become orientationally more ordered due to the aligning effect of longer rods if $1.5\pi / I_p < \rho^* < 5$. Opposite to this, the strongly ordered nematic phase of the monodisperse system becomes less ordered with increasing I_p due to the disordering effect of the shorter rods. This can be seen clearly in Fig. 4 for $\rho^* > 5$. Regarding the differences arising from the used distribution functions, we can see that the SF length distribution has a lower nematic order

parameter at high densities because it contains more short components than the LN one. Moreover, the nematic ordering is slightly stronger in the vicinity of the IN transition for the SF distribution than for LN one. In general, we can say that the trends are the same in S-ρ plane using SN and LN distributions. Therefore, we can conclude that higher nematic order can be realized in the monodisperse system than in the polydisperse one at high densities, while the onset of nematic ordering can be lowered in density with increasing polydispersity. The order of the IN phase transition turns out to be second-order for any possible value of I_p, which rules out the possibility of short needles accumulating in the isotropic phase and long needles in the

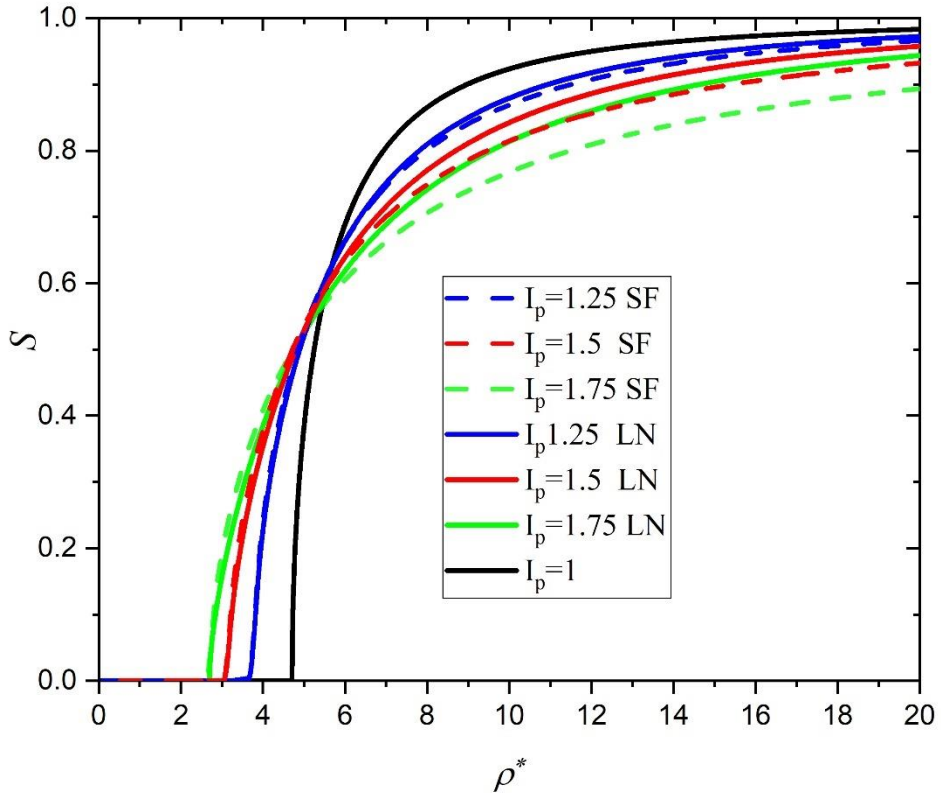

Figure 4: The global nematic order parameter as a function of 2D number density. The solid curve indicates the results of LN length distribution, while the dashed curve represents the results coming from SF one. The monodisperse (I_p=1) and the polydisperse I_p>1 systems are shown together.

nematic one. The length dependence of the nematic order parameter is presented for weakly nematic (ρ*=4 and S≈0.4) and strongly nematic (ρ*=8 and S≈0.7) cases in Fig. 5. We can see that very short rods (l*≈10^{-5}…10^{-3}) are weakly ordered, while the long ones (l*>5) are strongly

ordered in both cases. This shows that the ordering behavior of short and long rods is very different in the nematic phase. This is due to the fact that the competition between orientational and packing entropies results in an ordering where the parallel alignment of long rods increases packing entropy, while poorly aligned short rods are responsible for the gain in orientation entropy. This is reasonable because the excluded area between two long needles can be very high in perpendicular orientations, while it is zero for parallel one (see eq. (5)). Moreover, the parallel ordering of very short needles do not produce much extra room for the particles, but decreases the orientational entropy substantially. Therefore, the space available for particles can be better increased with long needles than with short ones, i.e. the long rods align strongly while the short ones weakly in the nematic phase. Although SF and LN distributions exhibit the same trends in Fig. 5, there is a slight difference between them. The SF produces higher nematic order than the LN one in the weakly nematic phase, while the opposite trend can be seen in the strongly ordered nematic phase. This difference is due to the different features of these two length distributions. In the inset of Fig. 5, we present the result of the optimized mixture optimization for the lengths and mole fractions, which are the input of Eq. (15). It can be seen that we must use more short components in the case of SF distribution, while more longer needles are needed in the case of LN one. However, these changes do not change the results substantially. We can say that even if the optimized mixture representation is different for SF and LN distributions, the results are not very sensitive to the choice of the distribution function applied for the length polydispersity. Therefore, we expect similar trends in the nematic ordering for other type of length distributions, which are not discussed here.

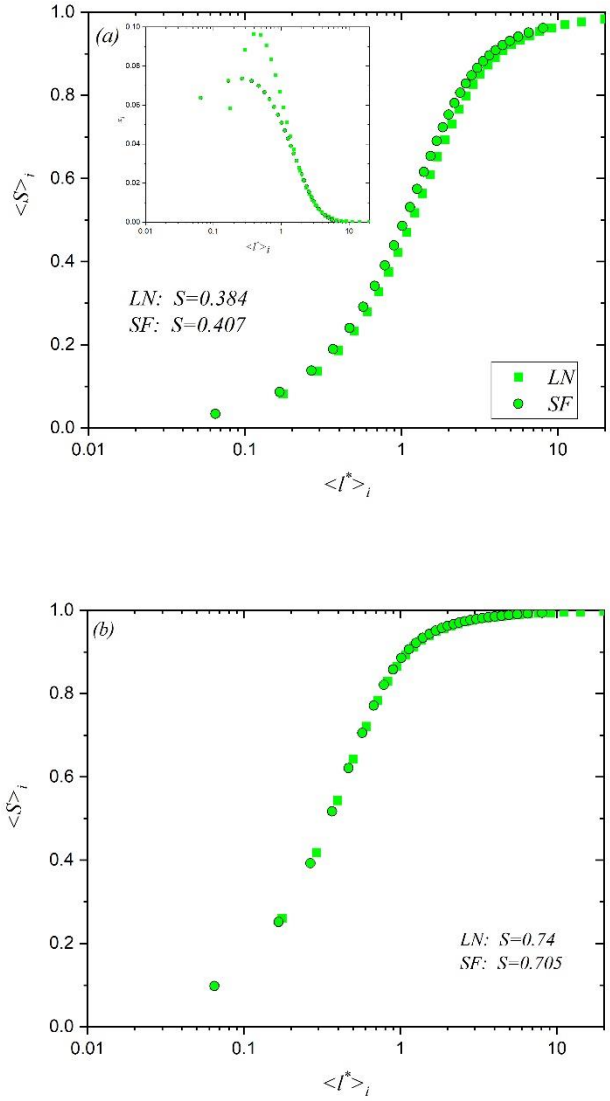

Figure 5: Nematic order parameter of hard needles as a function of length in weakly and strongly ordered nematic phases: (a) ρ^*=4 and (b) ρ^*=8 for I_p=1.75. Square and circle symbols represent the results for LN and SF length distribution functions, respectively. The insets show the mole fractions of the optimized mixture representation as a function of the lengths of the mixture, where n=30 for both distributions.

Conclusion

We have examined the effect of length polydispersity on the stability of the 2D nematic phase of hard needles using the Onsager theory. The ODF of the polydisperse needles has been determined with the help of a mixture optimization method, where the continuous system is considered as a n component mixture. In this method, the lengths and mole fractions of the components are chosen such that the polydispersity index of the mixture is as close as possible to the polydispersity index of the system having continuous polydispersity. This method allowed us to transform the inconvenient self-consistent equation of ODF into a numerically

tractable one. The advantage of the method is that it is enough to use only a few components to get reliable information about the effect of continuous distribution on the phase behavior of the polydisperse system. We found that there is no need to go beyond n=30 in the number of components even for very polydisperse cases to reproduce the properties of continuous distribution. In addition, the mixture optimization method can be extended easily for more complicated polydispersities depending on both diameter and length. This method can be particularly useful in future simulation studies, where the number of particles in the simulation box is finite.

We have shown that the density of isotropic-nematic transition is inversely proportional to I_p, i.e., polydispersity favors nematic ordering. This exact result holds for both discrete and continuous polydisperse systems. Interestingly, other features of the distribution have no effect on the transition density. Therefore, the isotropic-nematic phase transition takes place at the same density at a given value of I_p for all distributions such as constant, one-peaked, two-peaked, etc. length distributions. The shape of the distribution can, however, affect the degree of orientation ordering. It is found that both SF and LN distributions weaken the nematic ordering of the needles at high densities. We expect that this would also be the case for other distributions, as short rods always have more room to rotate than long ones. To get a different result, the order of the phase transition should change from second order to first one, where the short rods populate the isotropic phase, while the long ones are the nematic one. In this case, the nematic phase will be more ordered due to the absence of short rods responsible for the disorder. This really happens in the length polydisperse system of hard rectangles, where the polydispersity induces a first-order phase transition by a gap between the coexisting isotropic and nematic phases [50].

The connection of our work to the experiment is that the orientational ordering of hard needles is quite similar to that of semiconducting CNTs, which form a very ordered 2D nematic phase [15, 19]. The most important results of these experiments can be summarized as follows. a) The alignment of the nanotubes can be improved with increasing density and decreasing temperature [15]. b) The narrow length distribution produces the strongest nematic alignment [19]. From these findings, the polydisperse hard needle model captures the density and length distribution effects on the nematic ordering. However, the effect of temperate is not included in this model, because hard needles are athermal and the resulting phase behavior is independent of temperature. With the inclusion of dispersive interactions into the needle model, the effect of the temperature can be also examined. However, we believe that flexibility plays also a significant role in the nematic ordering because the shape of the nanotubes is not a straight line even if their average length is about 500 times longer than their average diameter. Therefore, we can only approximate the true shape of nanotubes with straight needles. Our attempts to compare the results of the theory with those of experiments failed because the nematic ordering occurs at densities at least an order of magnitude higher in experiments than in theory. This discrepancy of the needle model can be explained with the flexibility because the flexibility works against the nematic ordering and postpones the nematic ordering towards higher densities. Therefore, the hard needle model can only qualitatively reproduce part of the experimental results. To get deeper insight into the phase behavior of the 2D nematic phase of carbon nanotubes, the polydisperse hard needle model needs to be complimented with dispersive interactions and flexibility.

References

[1] S. Iijima, Nature **354**, 56 (1991).

[2] I. A. Kinloch, J. Suhr, J. Lou, R. J. Young, and P. M. Ajayan, Science **362**, 547 (2018).

[3] X. He et al., Nature Materials **17**, 663 (2018).

[4] A. Baydin, F. Tay, J. Fan, M. Manjappa, W. Gao, and J. Kono, Nano Lett. **18**, 4778 (2018).

[5] P. Avouris, J. Appenzeller, R. Martel, and S. J. Wind, Phys. Today **56**, 46 (2003).

[6] E. T. Thostenson, Z. Ren, and Tsu-Wei Chou, Comp. Science and Technology 61, 1899 (2001).

[7] T. Yamabe and K. Fukui, The Science and Technology of Carbon Nanotubes, Elsevier Inc., Amsterdam, Netherlands (1999).

[8] G. S. Tulevski, A. D. Franklin, D. Frank, J. M. Lobez, Q. Cao, H. Park, A. Afzali, S. J. Han, J. B. Hannon and W. Haensch, ACS Nano **8**, 8730 (2014).

[9] N. Puech, C. Blanc, E. Grelet, C. Zamora-Ledezma, M. Maugey, C. Zakri, E. Anglaret, and P. Poulin, Adv. Mater. **18**, 320 (2006).

[10] S. P. Yadav and S. Singh, Prog. Mater. Sci. **80**, 38 (2016).

[11] S. T. Beyer and K. Walus, Langmuir **28**, 8753-8759 (2012).

[12] I. Dierking, G. Scalia, P. Morales, and D. LeClere, Adv. Mater. **16**, 865 (2004).

[13] K. Ariga, J.P. Hill, M.V. Lee, A. Vinu, R. Charvet, and S. Acharya, Sci. Technol. Adv. Mater. **9**, 014109 (2008).

[14] A. Bravo-Sanchez, T.J. Simmons, and M.A. Vidal, Phys. Rev. Lett. **101**, 157801 (2008).

[15] K. R. Jinkins, S. M. Foradori, V. Saraswat, R. M. Jacobberger, J. H. Dwyer, P. Gopalan, A. Berson, and M. S. Arnold, Sci. Adv. 7, eabh0640 (2021).

[16] Y. Joo, G.J. Brady, M.S. Arnold, and P. Gopalan, Langmuir **30**, 3460 (2014).

[17] I. Baik et al., Appl. Phys. Lett. **87**, 263110 (2005).

[18] W. Zhou, J. E. Fischer, P. A. Heiney, H. Fan, V. A. Davis, M. Pasquali, and R. E. Smalley, Phys. Rev. B **72**, 045440 (2005).

[19] H. Wen et al., Nano Res. **16**, 1568 (2023).

[20] P. van der Schoot, V. Popa-Nita, and S. Kralj, J. Phys. Chem. B **112**, 4512 (2008).

[21] G. V. Varshini, D. S. Shankar Rao, P. K. Mukherjee, and S. K. Prasad, J. Phys. Chem. B **122**, 10774 (2018).

[22] M. Rahman and W. Lee, J. Phys. D: Appl. Phys. **42**, 063001 (2009).

[23] Y. Galerne, Phys. Rev. E **93**, 042702 (2016).

[24] S. B. Sumandra, B. Mahendra, F. Nugroho, and Y. Yusuf, Int. J. Comput. Mater. Sci. Eng. **11**, 2150033 (2022).

[25] T Lahiri, S. K. Pushkar, and P Poddar, Physica B: Condensed Matter **588**, 412177 (2020).

[26] P. K. Mukherjee, Soft Materials **17**, 321 (2019).

[27] S. P. Finner, I. Pihlajamaa, and P. van der Schoot, J. Chem. Phys. **152**, 064902 (2020).

[28] Y. Y. Tarasevich and A. V. Eserkepov, Phys. Rev. E **98**, 062142 (2018).

[29] J. Hicks, A. Behnam, and A. Ural, Phys. Rev. E **79**, 012102 (2009).

[30] P. Ma and H.K. Chan, Front. Phys. **9**, 778001 (2021).

[31] Y. Y. Tarasevich, I. V. Vodolazskaya, A. V. Eserkepov and R. K. Akhunzhanov, J. Appl. Phys. **125**, 134902 (2019).

[32] M. Majidian, C. Grimaldi, L. Forró and A. Magrez, Sci. Rep. **7**, 12553 (2017).

[33] L. Mederos, E. Velasco, and Y. Martínez-Ratón, J. Phys. Condens. Matter **26**, 463101 (2014).

[34] Z. Y. Chen, Phys. Rev. E **50**, 2849 (1994).

[35] A. M. Bohle, R. Hołyst, and T. Vilgis, Phys. Rev. Lett. **76**, 1396 (1996).

[36] M. A. Bates and D. Frenkel, J. Chem. Phys. **109**, 6193 (1998).

[37] N. Clarke, J. A. Cuesta R. Sear, P. Sollich and A. Speranza, J. Chem. Phys. **113**, 5817 (2000).

[38] S. Belli, A. Patti, M. Dijkstra, and R. van Roij, Phys. Rev. Lett. **107**, 148303 (2011).

[39] H. H. Wensink and G. J. Vroege, Phys. Rev. E **65**, 031716 (2002).

[40] H. H. Wensink and G. J. Vroege, J. Chem. Phys. **119**, 6868 (2003).

[41] C. A. De Filippo et al., Soft Matter **19**, 1732 (2023).

[42] D. Ioffe, Y. Velenik and M. Zahradník, J. Stat. Phys. **122**, 761 (2006).

[43] A. Speranza and P. Sollich, J. Chem. Phys. **117**, 5421 (2002).

[44] A. Speranza and P. Sollich, Phys. Rev. E **67**, 061702 (2003).

[45] A. Speranza and P. Sollich, J. Chem. Phys. **118**, 5213 (2003).

[46] R. F. Kayser and H. J. Raveché, Phys. Rev. A **17**, 2067 (1978).

[47] D. Frenkel and R. Eppenga, Phys. Rev. A **31**, 1776 (1985).

[48] S. Varga and I. Szalai, Mol. Phys. **95**, 515 (1998).

[49] The bifurcation analysis of Kayser and Ravaché can be extended to binary, ternary, etc. mixture. It is also possible to take the continuous limit.

[50] A. Díaz-De Armas and Y. Martínez-Ratón, Phys. Rev. E **95**, 052702 (2017).